Comparison of Approximations for the Analysis of Static and Dynamic Light Scattering Data from Distributions of Rodlike Polymers: Applications to Model Systems for Fibrin and Actin

Charles E. Montague

The Thomas C. Jenkins Department of Biophysics, The Johns Hopkins University, Baltimore, Maryland 21218

Jay Newman*

Department of Physics, Union College, Schenectady, New York 12308.
Received November 17, 1983

ABSTRACT: The applicability of various approximations used in the analysis of static and dynamic light scattering data from solutions of polydisperse rigid rodlike molecules is examined. Two length distributions were chosen for study: a version of the Flory–Stockmayer distribution which has been used to model fibrin polymerization, and an exponential number distribution which has been shown to represent the distribution of F-actin lengths at equilibrium. Calculations of the angular dependence of the scattered light intensity and the average decay rate constant, $\bar{\Gamma}$, were made by using the complete Pecora formulation and compared to those using approximations for the particle form factor, the diffusion coefficient, and the normalized field autocorrelation function for a rigid rod. Equations are presented to allow rapid numerical calculation of the autocorrelation function for rigid rods of any length. We show that linearity of Casassa plots at large values of the scattering vector, q, does not by itself (as is usually assumed) ensure the validity of the Casassa approximation for the form factor, nor does it ensure the accuracy of the derived mass-per-length. Also, a nearly linear plot of $\bar{\Gamma}$ vs. q^2 can result from a highly polydisperse solution of rods and is not evidence for a monodisperse sample.

Introduction

Static and dynamic light scattering techniques have been used to study many rodlike macromolecules. These have included various biopolymers, such as viruses,[1-3] collagen,[4] microtubules,[5] actin,[6-9] myosin,[10] native muscle thin filaments,[11] and fibrin,[12-17] as well as many synthetic polymers, e.g., poly(γ-benzyl L-glutamate) (PBLG).[18] In nearly all of these studies an analysis was performed that treated the molecule as a rigid rod. This was a useful analysis to perform even though other models that allowed for rod flexibility were also used. The theories for light scattering from monodisperse isotropic solutions of randomly oriented thin rigid rods were developed by Neugebauer[19] and Zimm[20] for the static case and by Pecora[21] for the dynamic case of isotropic diffusion. Pecora and Tagami[22,23] have considered the effects of length polydispersity in rigid rods on both the integrated and fluctuating scattered light intensity terms arising from the pure translational diffusion. Using a two-parameter, unimodal (Schultz) distribution of rigid rods they have shown that the shape of this distribution function has significant effects on both the integrated and fluctuating intensity terms.

Various approximations are often used for the particle form factor, $P(\theta)$, and for the full formulation of the field autocorrelation function, $g^{(1)}(\tau)$, for rigid rods. When these approximations are used in analyzing data from polydisperse systems, care must be taken to ensure that the length distribution of rods does not invalidate the approximations used. In this paper, we consider several generally useful approximations for $P(\theta)$ and $g^{(1)}(\tau)$ for rigid rods and illustrate their application to polydisperse systems. Distributions were chosen to simulate samples of (1) protofibrils early in the polymerization of fibrin and (2) actin filaments after reaching their equilibrium distribution. Casassa[12] pioneered static light scattering work on the fibrinogen–fibrin system in the mid-1950s. Wiltzius and co-workers[13-15] have recently analyzed, in some detail, both static and dynamic light scattering data on the fibrin system using the Flory–Stockmayer distribution. The second sample system studied, an exponential number distribution of actin filament lengths, was first investigated by Oosawa and co-workers[24,25] and more recently by Wegner[9,10] using static light scattering to provide details of the nucleation–elongation kinetics. Our considerations of these two contrasting distributions will illustrate some pitfalls in modeling and some general guidelines for the analysis of data for rigid rod systems.

Theory

Approximations for $P(\theta)$. The Rayleigh ratio, R_θ, of the light scattered by a dilute monodisperse solution of optically isotropic particles at an angle θ is[26]

$$R_\theta = KcMP(\theta) \tag{1}$$

where K equals $2\pi^2 n^2 (\mathrm{d}n/\mathrm{d}c)^2 / N_A \lambda_0^4$, c is the weight concentration of solute, M is the molecular weight, and $P(\theta)$ is the particle form factor. For a polydisperse solution, assuming $\mathrm{d}n/\mathrm{d}c$, the specific refractive index increment, is identical for all species, the generalization of eq 1 is

$$R_\theta = Kc \sum_i M_i f_{w,i} P_i(\theta) \tag{2}$$

where $f_{w,i}$ is the weight fraction of the ith species.

The form factor, $P(\theta)$, for randomly oriented, optically isotropic thin rigid rods of length L and diameter d can be calculated by using the Rayleigh–Debye approximation[19,27] to be

$$P(\theta) = (2/qL) \int_0^{qL} \frac{\sin(x)}{x}\,\mathrm{d}x - \left[\frac{\sin(qL/2)}{qL/2}\right]^2 \tag{3}$$

where q equals $4\pi n \sin(\theta/2)/\lambda_0$. The assumptions of the Rayleigh–Debye formulation are that $m - 1 \ll 1$ and $2\kappa L(m - 1) \ll 1$, where m is the relative refractive index of the scatterer and κ equals $2\pi n/\lambda_0$. A thin rod is one in which $d \ll \lambda_0/n$. Casassa[12] expanded eq 3 in a Taylor series in terms of $(qL)^{-1}$ to obtain the approximation

$$P_C(\theta) = \pi/qL - 2/(qL)^2 \tag{4}$$

which is valid for long thin rods (large qL). As qL increases further, the first term is sufficient, giving

$$P_L(\theta) = \pi/qL \tag{5}$$

0024-9297/84/2217-1391$01.50/0

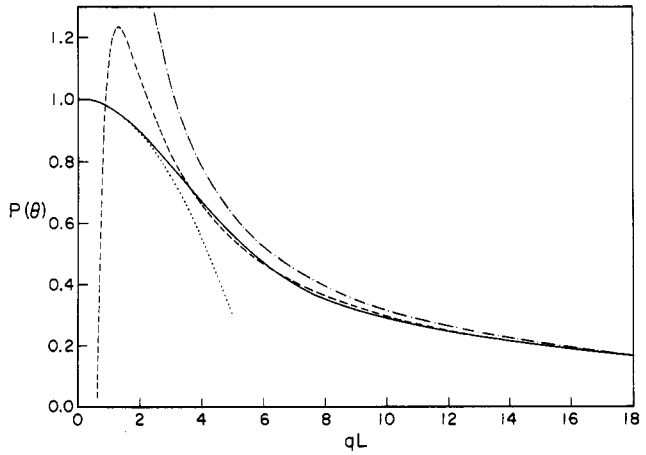

Figure 1. Form factor for rods, $P(\theta)$, and various approximations as functions of qL. The solid curve is the exact calculation (eq 3), the dashed curve is the Casassa approximation (eq 4), seen here to be valid for $qL \gtrsim 3$, the dot–dash curve is the π/qL approximation (eq 5) which, even at $qL = 8$ is 9% too large, and the dotted curve at small qL is the radius of gyration approximation (eq 6), valid for $qL \lesssim 3$.

Another approximation for $P(\theta)$, valid for any size or shape of particle in the limit of small scattering angles, is $P(\theta) = 1 - q^2R_g^2/3$, where R_g is the radius of gyration of the particle.[26] Substituting $R_g^2 = L^2/12$ for a thin rigid rod yields

$$P_R(\theta) = 1 - (qL)^2/36 \tag{6}$$

Figure 1 shows plots of eq 3–6. Equation 6 will not be treated further in this paper but has been included to provide an analytical approximation to $P(\theta)$ that is valid in the range of qL where the other approximations fail.

Approximations for $g^{(1)}(\tau)$. The normalized field autocorrelation function for a rigid rod is[21,28]

$$g^{(1)}(\tau) = e^{-D_T q^2}[\sum_{\substack{l=0 \\ \text{even}}}^{\infty} B_l(qL)e^{-l(l+1)D_R\tau}]/P(\theta) \tag{7}$$

where $B_l(qL)$ equals $(2l + 1)(2/qL)^2|\int_0^{qL/2} j_l(x)\,dx|^2$. The form factor can be written[28] as $P(\theta) = \sum_{l=0,\text{even}}^{\infty} B_l(qL)$, and D_T and D_R are the translational and rotational diffusion coefficients, respectively. This formulation assumes that the rods are optically isotropic and neglects the anisotropy of the translational and rotational diffusion coefficients. In the limit of small qL, $B_0(qL) \cong 1$, the rotational terms are negligible, and

$$g^{(1)}(\tau) \cong e^{-D_T q^2 \tau} \tag{8}$$

For a polydisperse sample, one can define a mean decay constant, $\bar{\Gamma}(q)$, to be[28]

$$\bar{\Gamma}(q) = \frac{\sum_i f_{w,i}M_iP_i(\theta)\Gamma_i(q)}{\sum_i f_{w,i}M_iP_i(\theta)} \tag{9}$$

where, in the case of rods,

$$\Gamma_i(q) = [\sum_{\substack{l \\ \text{even}}} B_l(qL_i)[D_{T,i}q^2 + l(l + 1)D_{R,i}]]/P_i(\theta) \tag{10}$$

$\bar{\Gamma}(q)$ and the corresponding effective diffusion coefficient, $\bar{D} = \bar{\Gamma}/q^2$, can be readily extracted from experimental data by an analysis using the method of cumulants.[29]

Specific Scattered Intensity.[50] The intensity of light scattered by a particle at a given angle increases proportionately with its mass but is modulated by intraparticle interference, as expressed in the particle form factor in eq 1. If a solution of such particles associates to form larger particles, the scattered intensity of the resulting particle is again a function of its mass, size, and shape. To quantify this scattered intensity, it is useful to introduce the notion of the relative scattered intensity per unit mass. We can define the specific scattered intensity, I_{sp}, to be the ratio of the intensity of light scattered by a solution to the intensity that would result from a solution of point scatterers with the same mass. For a thin rod, one can conceptually dissect the rod into cross-sectional elements of mass M_0 and length L_0 small enough such that $P(qL_0) = 1$. (For a rodlike polymer, the monomers can be equated to these elements only if the monomers are Rayleigh scatterers.) For this case, from eq 1, I_{sp} can be written as

$$I_{sp}(qL) = \frac{I_{rod}(qL)}{I_{Rayleigh}} = \frac{Kc[(L/L_0)M_0]P(qL)}{KcM_0} = \frac{LP(qL)}{L_0} \tag{11}$$

Using eq 5, one finds that for very long rods, I_{sp} approaches π/qL_0, which is independent of filament length.

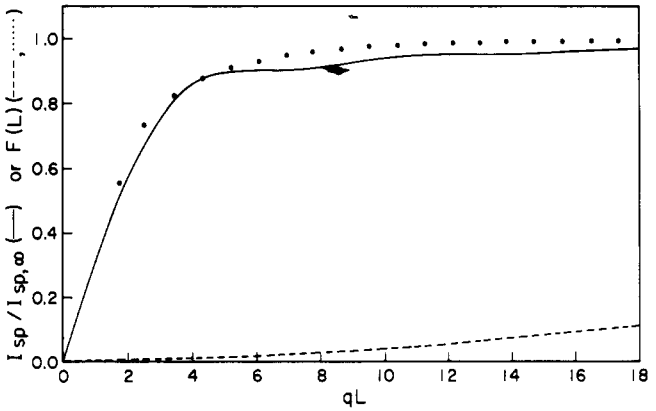

Figure 2. Normalized specific scattered intensity, $I_{sp}(qL)/I_{sp,\infty}$, for thin rods (solid curve). A similar plot has been presented in the specific context of a study on fibrin.[16] Also shown are the cumulative weight distributions, $F(L)$, for fibrin (●) and actin (---) plotted vs. a scaled length axis (corresponding to $\lambda_0 = 514.5$ nm and $\theta = 90°$). Both distribution curves are discrete; however, because of the small monomer size, the distribution curve for actin is drawn continuously. (The correspondence of the fibrin curve to the $I_{sp}/I_{sp,\infty}$ curve is coincidental.)

In Figure 2, the smooth curve is a plot of I_{sp} normalized by the specific scattered intensity for very long rods, $I_{sp}(\infty)$, as a function of qL. At a fixed value of q, this shows the length dependence of I_{sp}. The plateau in this curve above $qL \sim 5$ is due to the inverse proportionality of $P(\theta)$ on mass for rods. The fact that this curve plateaus is the basis for the wide use of total scattered intensity to follow the actin filament weight concentration in a polymerizing actin solution.[9,30]

Methodology of Model Calculations

For large values of qL, calculation of $\bar{\Gamma}$ to any reasonable precision requires retention of many B_l terms. For example, when $qL = 46$, corresponding to a 2-μm rod at 90° with $\lambda_0 = 5145$ Å, 15 terms are necessary before the increment in the total sum in eq 10 due to the last term is less than 1%. An increment of 1% or less was our criterion for truncating a series calculation. We found that as qL increased, an additional B_l term was required for every qL increment of about 4–5.

To allow calculation of $B_l(qL)$ for large values of l and qL, we have used iterative equations for the integrals of spherical Bessel functions[31]

$$j_{n+1}(z) = \frac{2n + 1}{z}j_n(z) - j_{n-1}(z)$$

$$\int_0^z j_{n+1}(x)\,dx = \frac{n}{n+1}\int_0^z j_{n-1}(x)\,dx - \frac{2n+1}{n+1}j_n(z)$$

Thus, starting with a simple numerical evaluation of integrals of j_0 and j_1, one can easily evaluate all higher orders.[50]

In order to evaluate eq 10, analytical expressions are needed for D_T and D_R. We have used the Broersma relations:[2,32-34]

$$D_T = \left(\frac{kT}{3\pi\eta L}\right)[\delta - \tfrac{1}{2}(\gamma_\parallel + \gamma_\perp)] \quad (12a)$$

$$D_R = \left(\frac{3kT}{\pi\eta L^3}\right)(\delta - \xi) \quad (12b)$$

with $\delta = \ln(L/r)$, $\gamma_\parallel = 1.27 - 7.4(1/\delta - 0.34)^2$, $\gamma_\perp = 0.19 - 4.2(1/\delta - 0.39)^2$, and $\xi = 1.45 - 7.5(1/\delta - 0.27)^2$. In the staggered overlap rod model an equal volume equivalent radius of $2^{1/2}r$ was used, where r is the subunit radius. The differences between calculations of D_T and D_R based on the above equations and those based on the equations of Tirado and de la Torre[35,36] are negligible for the range of rod axial ratios of interest here.

For certain particle shapes, over a limited range of molecular weights,[28] $D_T = CM^{-\beta}$. In the case of a homopolymer this can be written as

$$D_{T,i} = D_1(i)^{-\beta} \quad (13)$$

where D_1 is the translational diffusion coefficient of the monomer. For a linear polymer $i = L_i/L_1$, where L_1 is the monomer length. For the staggered overlap case that we will examine here, $i = L_i/L_1 - 1$. We have used a value of $\beta = 1$, as did Wiltzius et al.[13,14] This choice neglects the term in square brackets in eq 12A but, for a narrow size distribution, this correction is small.

Polydisperse Distributions. For the purpose of modeling polydisperse solutions of rods, two distributions were chosen that have been used to describe biological macromolecules. In both of these cases, the macromolecules have also been extensively studied by light scattering techniques. Wiltzius and co-workers[13] have used the Flory–Stockmayer distribution in the form

$$f_{w,i} = \frac{e^{-\lambda}(i\lambda)^{i-1}}{i!} \quad (14)$$

to describe the pregelation stages of fibrin polymerization. The parameter λ varies from 0, only monomer present, to 1, and i is the number of subunits in the polymer. Wiltzius et al.[19] modeled their data with $0 \le \lambda \le 0.9$. We have used the staggered overlap model that Wiltzius et al. found to be appropriate for fibrin. We have chosen two values of λ in this range, 0.6 and 0.9, to present for comparison with their results. The results presented below are qualitatively unchanged even at values of λ approaching 1.

The appropriate distribution for a condensation polymerization reaction is[37]

$$f_{w,i} = i(1-P)^2P^{i-1} \quad (15)$$

where P represents the fraction of monomers that has reacted. We will refer to this distribution as an exponential distribution, since the number fraction is proportional to $\exp(i \ln(P))$. Actin polymerization is generally considered to be a condensation reaction, coupled to a nucleation step. This leads to a fixed concentration of monomers, the critical concentration, which is a function of solvent conditions, with the distribution of remaining molecules being described by an exponential distribution.[38] From the exponential distribution, one can derive expressions for the weight- and number-averaged filament length, $\langle L\rangle_w$ and $\langle L\rangle_n$, respectively. Using these expressions and average lengths taken from the literature,[39,40] we obtain values of P clustered tightly around 0.998.

Qualitatively the nature of these two weight distributions is very different. For all values of λ, the predominant species in the Flory–Stockmayer distribution is the monomer. In comparison, the most probable species in the exponential distribution is the 500-mer. Cumulative weight distributions, $F_n = \sum_1^n f_{w,i}$ for these two cases are shown in Figure 2.

Results and Discussion

We now consider various approximations for the analysis of static light scattering data obtained from polydisperse solutions using the model systems discussed above. The results presented below apply only to systems of rigid rods. Consequently, a direct comparison with experimental results may be complicated by flexibility of these macromolecules. For F-actin, persistence length estimates range upward from 6.5 μm.[41] From eq 15 with $P = 0.998$, it can be determined that less than 5% by weight (0.8% by number) of the F-actin has lengths greater than one persistence length. This implies that any contribution to the light scattering from rod flexibility is probably small.

For our model of the fibrin system the monomer is the predominant species, even at high degrees of polymerization, constituting about 55%, 41%, and 37% by weight at $\lambda = 0.6$, 0.9, and 1.0, respectively. The fibrinogen monomer is a rodlike macromolecule itself with a length of 75 nm.[15] From this length and a D_T value of 1.95×10^{-7} cm^2/s for fibrinogen,[13] eq 12A yields an effective hydrodynamic diameter of 2.5 nm. In Figure 3A, we show the dependence of the inverse scattered intensity, I^{-1}, on the magnitude of the scattering vector, q, for different values of λ. This type of plot has been called a Casassa or Holtzer plot although one must distinguish this plotting procedure from the Casassa approximation discussed above. As λ increases, the plots become more linear and the Casassa approximation improves. From Figure 1 it can be seen that at $qL = 1.7$, the value for the monomer at an angle of 90°, the Casassa approximation for $P(\theta)$ is about 20% too high. Since at all values of λ the monomer is by far the dominant species by weight and, as Figure 2 indicates, the scattering per unit mass from long rods (those with $qL \gtrsim 5$) does not increase significantly, the failure of the Casassa approximation for $qL \lesssim 3$ is the essential cause of the deviation of the approximation curves from the corresponding correct results in Figure 3A. The Casassa approximation deviates from the correct result not only at low angles (where it would fail even in the absence of monomer) but at higher angles as well because the weight distribution is heavily skewed toward the monomer.

The Casassa approximation for $P(\theta)$ leads to an expression for $I^{-1}(q)$ that allows the weight-averaged mass-per-length to be determined from the slope of a plot of $I^{-1}(q)$ vs. q at large values of q. In Figure 3A, all the curves can be reasonably well approximated by straight lines at high q. The π/qL approximation (used by previous workers[13,14,42]) is a very poor approximation to $P(\theta)$ for this system. Even though the $P(\theta)$ curves at high q are linear, they underestimate the actual weight-averaged mass-per-length by 62%, 23%, and 12% at $\lambda = 0$, 0.6, and 0.9, respectively. Thus if experimental data (solid curves in Figure 3A) which are correctly modeled by the Flory–Stockmayer distribution were analyzed and interpreted with the Casassa or the π/qL approximation, the mass-per-length values obtained from the linear portion of the curve would be systematically in error.

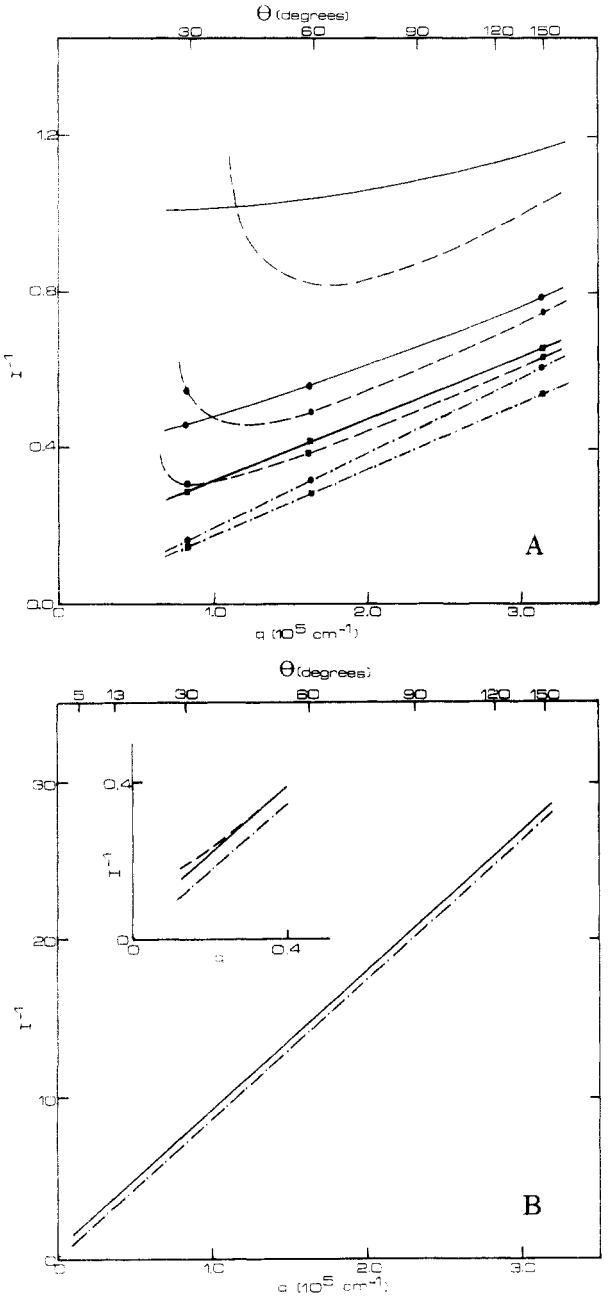

Figure 3. (A) Casassa plot for the fibrin model. The solid curves are the full $P(\theta)$ calculations (eq 3), the dashed curves are those for the Casassa approximation (eq 4), and the dot–dash curves are those for the π/qL approximation (eq 5), as applied to the fibrin system for $\lambda = 0$ (unlabeled curves), $\lambda = 0.6$ (●), and $\lambda = 0.9$ (■). (B) Similar plot for the actin model. The solid curve is the full $P(\theta)$ calculation, the dashed curve is for the Casassa approximation and is coincident with the solid curve except in the insert, which is an enlargement of the low-q region, and the dot–dash curve is for the π/qL approximation. We have assumed a protein concentration of 1 mg/mL and a critical concentration of 5 μg/mL.

Figure 3B shows a similar plot for the exponential number distribution of actin. This distribution differs from the Flory–Stockmayer distribution in several significant respects (see Figure 2). Less than 2% by weight of F-actin is shorter than 0.25 μm (with a qL value of 6.5 at a scattering angle of 90°). This contrasts with the ~95% by weight of fibrin rods with $qL \lesssim 6.5$. The actin weight distribution peaks at 1.4 μm, with a corresponding value of qL equal to 30 at 90°. Almost 40% of the weight concentration of actin is from filaments longer than 3 μm, while the corresponding fraction for the Flory–Stockmayer distribution, even at $\lambda = 0.9$, is less than 1%. Because of the paucity of F-actin with $qL \lesssim 3$, the Casassa approximation would be expected to hold quite well for actin. That this is the case is shown in Figure 3B, where the deviation of the Casassa approximation from the true $P(\theta)$ is seen to be less than 3.5% at a scattering angle of 5° (see insert in Figure 3B). The slope of I^{-1} vs. q leads to the correct value of the weight-averaged mass-per-length.

The analysis and interpretation of dynamic light scattering data obtained from polydisperse rodlike samples require consideration not only of the form factor but also of the relative contributions from decay constants involving both translational and rotational diffusive motion. We now consider the applicability of various approximations for $g^{(1)}(\tau)$ to our model systems. Figure 4A is a plot of $\bar{D}$ vs. q^2 for the rigid rod model and the various approximations discussed above as applied to the fibrin model. The insert shows two of the curves redrawn as the corresponding decay rates, $\bar{\Gamma} = \bar{D}q^2$, which is a common but much less informative method of presenting this type of experimental data. Above 45° ($q^2 = 1.6 \times 10^{10}$ cm^{-2}), all of the curves involving approximations are within 20% of the exact rigid rod model curve.

For the complete rigid rod model of Pecora, the curve extrapolates at $q = 0$ to the z-averaged translational diffusion coefficient. For short rods, $qL \lesssim 1$, $\bar{D}$ is essentially independent of q. The curvature at higher q is due to two effects that result from longer rods. First, as q increases, the relative contribution to the total scattered intensity from the larger rods decreases due to intraparticle interference. This effectively increases the contribution to $\bar{D}$ from shorter rods, which have larger diffusion coefficients. Second, for a given length rod, the effective Γ_i increases as larger q values require contributions from rotational diffusion (see eq 10).

If the rotational terms, those with $l \neq 0$ in eq 10, are omitted, a curve is obtained (△) that agrees with the exact rigid rod calculation at low q as expected but that deviates increasingly from the correct curve as q increases. Thus it is apparent that the prominent slope in the correct curve at high q is due to contributions from rotational diffusion. The calculations that use the Casassa approximation with either the Broersma (●) or $D_1 i^{-1}$ (○) translational diffusion coefficients fail at the low angles (note points at $q^2 = 0.08 \times 10^{10}$ cm^{-2}) because of the failure of the form factor at low q (see Figure 1). For the approximation of $P_i(\theta) = \pi/qL_i$ and $D_{T,i} = D_1 i^{-1}$, not only is rotational diffusion neglected, but this particular form factor leads to a weighting function for Γ_i values in eq 9 that is independent of q.

Wiltzius et al.[14] derive an approximation formula for the $\bar{D}$ for a polydisperse solution of rodlike scatterers with $qL \gtrsim 1.5$. Our angle-independent approximation corresponds to their approximation, except that we have considered the rod in the staggered overlap model. Above 75°, at which qL for the monomer is 1.5, all of the approximations are accurate to within ~10%. Similar results are obtained for $\lambda = 0.9$. The neglect of the rotational diffusion contribution to $\bar{D}$ has relatively little effect here because of the large weight fraction of short rods. For example, when $\lambda = 0.6$, 90% by weight of the polymer is due to rods shorter than hexamers, with a maximum qL of 8 at an angle of 150°. A calculation of the contribution from translational diffusion alone ($l = 0$) to the partial sum up to hexamer in the numerator of eq 9 shows it to be more than 94%.

The situation for distributions of F-actin is quite different. Figure 4B shows analogous plots of $\bar{D}$ and $\bar{\Gamma}$ for an exponential distribution of F-actin. The general shapes

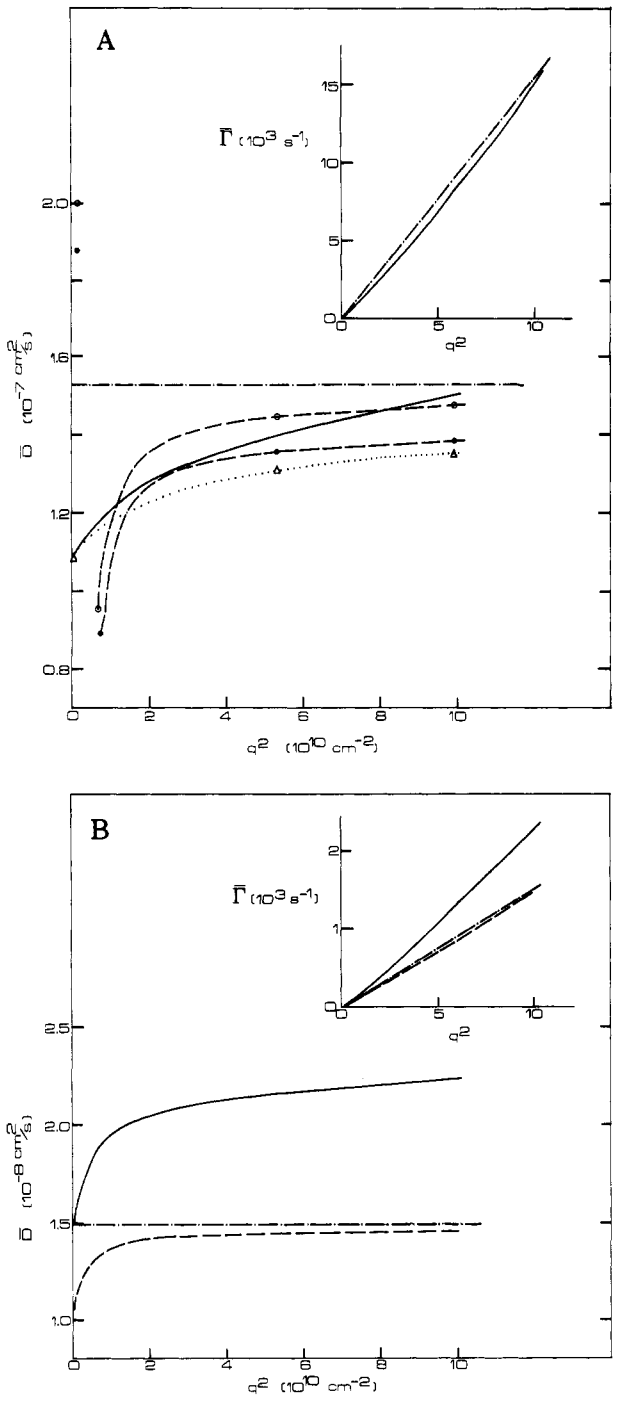

Figure 4. (A) q^2 angle dependence of the average diffusion coefficient for the fibrin model with $\lambda = 0.6$. The full rigid rod calculation (eq 9 with 10, 12, and 3) is shown as the solid curve, the same calculation neglecting rotational diffusion (eq 9 with 10 [$l = 0$ only], 12 and 3) is shown as the dotted curve (△), the Casassa and Broersma approximation (eq 9 with 10 [$l = 0$ only], 12A, and 4) is dashed and labeled (●), and the Casassa and $D_{T,i}$ approximation (eq 9 with 10 [$l = 0$ only], 13 and 4) is dashed and labeled (○). Note the displaced data points at $q^2 = 0.08 \times 10^{10}$ cm^{-2} resulting from the poor approximations at small q. The angle-independent π/qL and $D_{T,i}$ approximation (eq 9 with 10 [$l = 0$ only], 13, and 5) is shown as the dot–dash line. The insert shows two of these sets of data plotted as decay rates. (B) Similar plot for the actin model. The full rigid rod calculation is shown as the solid curve, the Casassa and Broersma approximation is the dashed curve, and the π/qL and Broersma approximation (eq 9 with 10 [$l = 0$ only], 12A, and 5) is shown as the dot–dash line. The $D_{T,i}$ approximation (not shown) for the translational diffusion coefficient is poor in this case, since the monomer is globular and not at all rodlike. The insert shows these data plotted as decay rates. Concentrations are as in Figure 3B.

of the curves are similar to the corresponding curves for the fibrin model. However, in this case the contribution to $\bar{D}$ from terms containing the rotational diffusion coefficient (those with $l \neq 0$ in eq 10) is quite large, leading to significant error in the approximations. For example, at a scattering angle of 90° about 87% of the total $\bar{D}$ value comes from terms with $l \neq 0$. From Figure 3B it is clear that the error is not due to the form factor approximation, which is quite good, but rather to the large neglected contribution from rotational diffusion. At 90°, more than half of the contribution to $\bar{D}$ comes from the 27% by weight (63% by number) shortest rods, those with lengths $L \lesssim 1.4$ μm or $qL \lesssim 32$. The longest 10% by weight rods (2% by number), those with $L \gtrsim 5.5$ μm or $qL \gtrsim 125$, contribute only about 3% to $\bar{D}$. This is surprising since the contribution of rods of a given length to the scattered intensity is proportional to their weight concentration for long rods. As a consequence of this, for the 98% of the filament mass with $qL \gtrsim 5$ the weighting function for Γ_i in eq 9 is simply the weight fraction, $f_{w,i}$. The explanation for the disproportionately small contribution of the longest rods to $\bar{D}$ lies in the strong inverse dependence of Γ_i on the length.

Conclusions

A study of various approximations for the static and dynamic light scattering from two contrasting model systems of rods has been presented. The results show that for the actin model, even the simplest approximation, π/qL, for the form factor is extremely accurate to below an angle of 10°. On the other hand, even at angles as small as 10°, the neglect of rotational diffusion would result in a 40% overestimate of the assumed z-averaged translational diffusion coefficient. In contrast, the neglect of rotational terms in the analysis of the fibrin model leads to at most a 10% error even at high angles. For this model, however, approximation for $P(\theta)$ leads to significant error in the interpretation of static light scattering data, which are a strong function of scattering angle and degree of polymerization. This is a general finding; that is, for rodlike systems where qL is large enough to justify the use of the Casassa or π/qL approximations for $P(\theta)$, significant contributions to the autocorrelation function result from rotational motions. Conversely, for systems in which qL is small enough so that rotational diffusion can be neglected, the Casassa and π/qL approximations for $P(\theta)$ fail.

A plot of the specific scattered intensity vs. qL has been very useful in determining the contributions of different length fractions to both the static and dynamic light scattering results presented above. The specific scattered intensity, as defined here, incorporates both the particle mass and the intraparticle interference effects on the scattered intensity. The fact that, for rigid rods, this parameter becomes independent of qL above $qL \sim 5$ is graphic justification for the use of total scattered light intensity for the measurement of weight concentrations of long filaments. This type of analysis is easily extended to other particle shapes and could prove useful in corresponding light scattering studies.

Analysis of the fibrin model shows that although Casassa plots may be linear at high q, a weight-averaged mass-per-length derived from the slope may have significant error. Thus, linearity of Casassa plots at high q does not ensure validity of the Casassa approximation.

Both of these models result in nearly linear plots of $\bar{\Gamma}$ vs. q^2. This result is often interpreted to imply that the sample under study is monodisperse. In our examples, this is obviously an incorrect interpretation. For polydisperse samples we strongly suggest that, since most of the vari-

ation of $\bar{D}$ occurs at small q and is obscured in a $\bar{\Gamma}$ vs. q^2 plot, such data be plotted as $\bar{\Gamma}/q^2$ vs. q^2.

The dynamic light scattering calculations in this paper are based on the theory of Pecora, which neglects the anisotropy of the translational and rotational diffusion coefficients. Although this problem has been addressed by several authors,[3,43-45] there is, as yet, no complete treatment that includes these terms. Wilcoxon and Schurr[43] have considered the dependence of the first cumulant of the dynamic scattering factor (which corresponds to $\bar{D}$ (and $\bar{\Gamma}$ in this work)) on the anisotropy of the translational diffusion coefficient ($\Delta = D_{\parallel} - D_{\perp}$) for a monodisperse solution of rods of length L. They show that for $qL \gg 1$, $\bar{\Gamma}$ becomes independent of $D_{\parallel}$. The error in neglecting this is small for the fibrin system, but due to the much larger actin filaments (cf. Figure 2), a systematic error is introduced into the calculations for actin. The magnitude of this error is at most $\Delta/3$. At the largest values of qL that are considered here, the longest rods would have a D (and Γ) overestimated by 15%. The effect on $\bar{D}$ and $\bar{\Gamma}$ for polydisperse distributions is less than 15% since the correction for anisotropy decreases for shorter rod lengths and, as we have shown, longer rods contribute disproportionately less to $\bar{D}$ and $\bar{\Gamma}$ than shorter rods.

An unusual feature of the analysis of the dynamic light scattering from the actin model is the need to include a large number of $B_i(qL)$ terms. To this end a useful recursion relation was developed. Modeling experimental data with an insufficient number of such terms will lead to a calculation of $\bar{\Gamma}$ that is systematically below the experimental value determined by the method of cumulants, even for a monodisperse solution of long rods. In considering the q^2 dependence of such data, one might mistakenly attribute this deviation to flexibility of the rod.

This study reinforces the point that a knowledge of the length distribution of rodlike systems is required before assuming the validity of any approximation scheme. Although length distributions can be determined by other physical techniques, such as electron microscopy, new methods of analysis of light scattering data have been and are being developed for this purpose.[46] Kuboto and Chu[47] have recently performed the first such analysis for rodlike particles. One of us (C.E.M.) has developed a technique based on the exponential sampling method[48] for direct extraction of the length distribution from polydisperse actin solutions.[49]

Acknowledgment. We thank F. D. Carlson for stimulating discussions and for critical reading of the manuscript. We also thank Nancy Hiss for drawing the figures. A portion of this work was performed in the laboratory of Dr. F. D. Carlson and supported by Grant 2R01AM 12803 from the USPHS to F. D. Carlson.

References and Notes

(1) Newman, J.; Day, L. A.; Dalack, G. W.; Eden, D. *Biochemistry* **1982**, *21*, 3352–3358.
(2) Newman, J.; Swinney, H. L.; Day, L. A. *J. Mol. Biol.* **1977**, *116*, 593–606.
(3) Loh, E.; Ralston, E.; Schumaker, V. N. *Biopolymers* **1979**, *18*, 2549–2567.
(4) Fletcher, G. C. *Biopolymers* **1976**, *15*, 2201–2217.
(5) Gethner, J. S.; Gaskin, F. *Biophys. J.* **1978**, *24*, 505–515.
(6) Carlson, F. D.; Fraser, A. B. *J. Mol. Biol.* **1974**, *89*, 273–281.
(7) Maeda, T.; Fujime, S. *J. Phys. Soc. Jpn.* **1977**, *42*, 1983–1991.
(8) Herbert, T. J.; Carlson, F. D. *Biopolymers* **1971**, *10*, 2231–2252.
(9) Wegner, A.; Engel, J. *Biophys. Chem.* **1975**, *3*, 215–225.
(10) Wegner, A. *J. Mol. Biol.* **1976**, *108*, 139–150.
(11) Newman, J.; Carlson, F. D. *Biophys. J.* **1980**, *29*, 37–48.
(12) Casassa, E. F. *J. Chem. Phys.* **1955**, *23*, 596–597.
(13) Wiltzius, P.; Dietler, G.; Känzig, W.; Hofmann, V.; Häberli, A.; Straub, P. W. *Biophys. J.* **1982**, *38*, 123–132.
(14) Wiltzius, P.; Dietler, G.; Känzig, W.; Häberli, A.; Straub, P. W. *Biopolymers* **1982**, *21*, 2205–2223.
(15) Wiltzius, P.; Känzig, W.; Hofmann, V.; Straub, P. W. *Biopolymers* **1981**, *20*, 2035–2049.
(16) Hantgan, R. R.; Hermans, J. *J. Biol. Chem.* **1979**, *254*, 11 272–11 281.
(17) Palmer, G. R.; Fritz, O. G. *Biopolymers* **1979**, *18*, 1659–1672.
(18) Kubota, K.; Chu, B. *Biopolymers* **1983**, *22*, 1461–1487.
(19) Neugebauer, T. *Ann. Phys.* **1943**, *42*, 509.
(20) Zimm, B. H.; Stein, R. S.; Doty, P. *Polym. Bull.* **1945**, *1*, 90.
(21) Pecora, R. *J. Chem. Phys.* **1968**, *48*, 4126–4128.
(22) Tagami, Y.; Pecora, R. *J. Chem. Phys.* **1969**, *51*, 3293–3298.
(23) Pecora, R.; Tagami, Y. *J. Chem. Phys.* **1969**, *51*, 3298–3305.
(24) Oosawa, F.; Kasai, M. In "Subunits in Biological Systems, Part A"; Timasheff, S. N., Fasman, G. D., Eds.; Dekker: New York, 1971.
(25) Oosawa, F.; Asakura, S. "Thermodynamics of the Polymerization of Protein"; Academic Press: New York, 1975.
(26) Tanford, C. "Physical Chemistry of Macromolecules"; Wiley: New York, 1961.
(27) Kerker, M. "The Scattering of Light and Other Electromagnetic Radiation"; Academic Press: London, 1969.
(28) Berne, B. J.; Pecora, R. "Dynamic Light Scattering with Applications to Chemistry, Biology and Physics"; Wiley: New York, 1976.
(29) Koppel, D. *J. Chem. Phys.* **1972**, *57*, 4814–4820.
(30) Cooper, J. A.; Pollard, T. D. In *Methods Enzymol.* **1982**, *85B*, 182–210.
(31) Arfken, G. "Mathematical Methods for Physicists"; Academic Press: London, 1970.
(32) Broersma, S. *J. Chem. Phys.* **1960**, *32*, 1626–1631.
(33) Broersma, S. *J. Chem. Phys.* **1960**, *32*, 1632–1635.
(34) Broersma, S. *J. Chem. Phys.* **1981**, *74*, 6989–6990.
(35) Tirado, M. M.; Garcia de la Torre, J. *J. Chem. Phys.* **1979**, *71*, 2581–2587.
(36) Tirado, M. M.; Garcia de la Torre, J. *J. Chem. Phys.* **1980**, *73*, 1986–1993.
(37) Flory, P. J. "Principles of Polymer Chemistry"; Cornell University Press: Ithaca, NY, 1953.
(38) Oosawa, F. *J. Theor. Biol.* **1970**, *27*, 69–86.
(39) Yin, H. L.; Zaner, K. S.; Stossel, T. P. *J. Biol. Chem.* **1980**, *255*, 9494–9500.
(40) Kawamura, M.; Maruyama, K. *J. Biochem.* **1970**, *67*, 437–457.
(41) Takabayashi, T.; Morita, Y.; Oosawa, F. *Biochim. Biophys. Acta* **1977**, *492*, 357–363.
(42) Müller, M.; Burchard, W. *Int. J. Biol. Macromol.* **1981**, *3*, 71–76.
(43) Wilcoxon, J.; Schurr, J. M. *Biopolymers* **1983**, *22*, 849–868.
(44) Maeda, H.; Saito, N. *J. Phys. Soc. Jpn.* **1969**, *27*, 984–991.
(45) Schaefer, D. W.; Benedek, G. B.; Schofield, P.; Bradford, E. *J. Chem. Phys.* **1971**, *55*, 3884–3895.
(46) Dahneke, B. E., Ed. "Measurement of Suspended Particles by Quasi-Elastic Light Scattering"; Wiley: New York, 1983.
(47) Kubota, K.; Chu, B. *Biopolymers* **1983**, *22*, 1461–1487.
(48) Ostrowsky, N.; Sornette, D.; Parker, P.; Pike, E. R. *Opt. Acta* **1981**, *28*, 1059–1070.
(49) Montague, C. E.; Carlson, F. D., in preparation.
(50) Montague, C. E. Ph.D. Thesis, Johns Hopkins University, 1984.